European Journal of Environmental and Civil Engineering

Volume 27 Number 12 October 2023

Taylor & Francis
Taylor & Francis Group

ISSN: 1964-8189 (Print) 2116-7214 (Online) Journal homepage: www.tandfonline.com/journals/tece20

Effects of hydration mechanism on mechanical properties of diatomite-cement composites

Yilmaz Kocak & İbrahim Pınarcı

To cite this article: Yilmaz Kocak & İbrahim Pınarcı (2023) Effects of hydration mechanism on mechanical properties of diatomite-cement composites, European Journal of Environmental and Civil Engineering, 27:12, 3707-3721, DOI: 10.1080/19648189.2022.2147099

To link to this article: https://doi.org/10.1080/19648189.2022.2147099

Published online: 21 Nov 2022.

EUROPEAN JOURNAL OF ENVIRONMENTAL AND CIVIL ENGINEERING
2023, VOL. 27, NO. 12, 3707–3721
https://doi.org/10.1080/19648189.2022.2147099

Effects of hydration mechanism on mechanical properties of diatomite-cement composites

Yilmaz Kocak[a] and İbrahim Pınarcı[b]

[a]Department of Civil Engineering, Faculty of Engineering, Duzce University, Duzce, Turkey; [b]Department of Design, Pazaryeri Vocational School, Bilecik Seyh Edebali University, Bilecik, Turkey

ABSTRACT

In this study, the relationships among compressive strengths with hydration mechanisms, microstructure characterizations and physical properties of diatomite-substituted cement pastes and mortars were researched. In order to determine the properties of cement pastes and mortars, X–ray diffraction, fourier transforms infrared spectroscopy, thermal analysis, scanning electron microscopy and energy dispersive X-ray spectroscopy techniques and standard cement tests were utilized at 2, 7, 28 and 90 days. The results revealed that portlandite content decreased gradually as a consequence of increasing age and addition of diatomite, and diatomite-substituted cements have high degree of hydration. Furthermore, the diatomite substituted cements had more compact structure by creating more hydration products at 28 and 90 days. This compact structure also positively contributed to the compressive strength of cement mortars at later ages.

ARTICLE HISTORY
Received 30 August 2022
Accepted 7 November 2022

KEYWORDS
Diatomite; Portland cement; microstructure; hydration; compressive strength

1. Introduction

Use of high volumes of supplementary cementitious materials reduces the demand for cement in the construction sector, thus decreases the cost of concrete production and decreases the environmental pollution owing to the CO_2 emission from the cement factories (Hasanbeigi et al., 2012; Sarı et al., 2020). In addition, in the cement and concrete business, supplemental cementitious ingredients are commonly employed as they contribute to strength and durability of concrete (Ashraf et al., 2022; Chen et al., 2018; Gerengi et al., 2017; Lei & Zhang, 2021; Tran et al., 2019). For this reason, trass (Kocak, 2017), pumice (Pınarcı & Kocak, 2022), zeolite (Akbarpour & Mahdikhani, 2022), silica füme (Mastali & Dalvand, 2018), blast furnace slag (Lenka et al., 2022), fly ash (Ganeshan & Venkataraman, 2021), metakaolin (Kocak, 2020), rice husk ash (Sandhu & Siddique, 2022) etc. are extensively used cement and concrete technology.

One of the most widely can also be used types of cement–based materials is diatomite which is among the most abundant minerals. Diatomite is a siliceous rock including amorphous and fine silica particles that are formed due to accumulation of shells or skeletons of fossilized ruins of single-celled aquatic algae and microscopic particles named diatoms (Ahmadi et al., 2018). Diatomite is an excellent natural material with high adsorption capacity, polymorphic, very high porosity, low density, high purity (Liu et al., 2021; Wen et al., 2018). These excellent properties of diatomite make it suitable for many industrial and scientific purposes. In this context, diatomite is also pozzolanic material extensively used for partial substitution of cement in the manufacture of concrete due to the excellent the physical structure and chemical composition and gives many useful properties to cement and concrete properties.

CONTACT Yilmaz Kocak yilmazkocak@hotmail.com Department of Civil Engineering, Faculty of Engineering, Duzce University, Duzce 81620, Turkey.

With the use of diatomite in concrete is reduced the permeability by contributing to the formation of hydrated products in higher amounts, in this way, the level of corrosion resistance and durability of concrete is increased (Kastis et al., 2006; Kurtay et al., 2020; Liu et al., 2017; Paiva et al., 2017). In addition, diatomite positively affects the sulfate resistance, freezing and thawing resistance properties (Degirmenci & Yilmaz, 2009; Sun et al., 2020). Furthermore, with the use of diatomite significant reductions in CO_2 emission, lower global warming potential and energy use is provided (Lauermannová et al., 2021; Li et al., 2019; Pokorny et al., 2019).

Using diatomite as an additive to cement may not only decreases the amount of cement and improve durability parameters but can also cause positive alterations in micro-structural by contributing to the formation of higher amounts of C–S–H. Cement and pozzolanic materials have complex hydration reactions, and it is not possible to determine the chemical reactions that arise in the formations of the materials with only one method. Because cement and pozzolans both have complex hydration reactions, it is not possible to determine the chemical reactions that take place in the structures of the materials with a single method. For this reason, supplement techniques such as X–ray diffraction (XRD), fourier transforms infrared spectroscopy (FT–IR), scanning electron microscopy and energy dispersive X-ray spectroscopy (SEM/EDS) and thermal (DTA/TGA) analysis, to explore complex hydration reactions were used in the study. Furthermore, the compressive strengths, water demand, initial and final setting time and volume expansion of Portland cement and diatomite-substituted cement mortars and pastes were investigated with standard cement tests.

2. Materials and methods

2.1. Materials

CEM I 42.5 R type Portland cement was used in the study. Blaine, specific weight, residue on 90 and 45 μm sieve of the Portland cement (PC) are 3822 cm^2/g, 3.18 g/cm^3, 0% and 3.2%, respectively. Diatomite powder was obtained from EP mineral company. The specific surface area, specific weight, residue on 90 and 45 μm sieve of diatomite (D) are 6112 cm^2/g, 2.58 g/cm^3, 0% and 0.1%, respectively. The sand in conceit with TS EN 196-1 (2016), and regular tap water of the province of Eskisehir were used to manufacture mortars.

The chemical composition of the PC and diatomite detected by XRF analysis (ARL 9900 Intellipower X–ray Analyzer) are given in Table 1. According to Table 1, diatomite is mostly composed of silicon dioxide (SiO_2), and the mass fractions of $SiO_2+ Al_2O_3+ Fe_2O_3$ are 88.75% for diatomite. This complies with the stated requirements ($SiO_2+ Al_2O_3+ Fe_2O_3>70\%$) for a natural pozzolan (TS 25, 2015; ASTM C 618, 2003).

Images of XRD patterns, FT–IR diagram, SEM micrograph and EDS spectra of diatomite are shown in Figure 1.

In accordance with the XRD patterns of diatomite, the broad reflection in the range of $2\theta = 15–38^\circ$ is ascribed to the amorphous silica (glassy form), and the peaks at $2\theta = 21.76^\circ$, 27.61° and 34.86° are attributed to quartz (Figure 1a) (Figarska-Warchoł et al., 2015; Yao et al., 2018).

Figure 1b presents the FT-IR spectra of diatomite. As also seen from Figure 1b the stretching vibration band at 3388 cm^{-1} and the weak bending vibration band at 1633 cm^{-1} can be attributed to the O-H group of water in diatomite. The intense band at 1066 cm^{-1} indicates to the stretching vibration of Si–O–Si group. The band at 798 cm^{-1} belongs the vibration of SiO–H group. The peaks at 448 and 551 cm^{-1} are associated with the Si-O bending vibration mode (Figure 1b). These characteristic peaks determined as a result of FT-IR analysis show that diatomite is chiefly formed of SiO_2 (Costa et al., 2020; Qian et al., 2015; Sarı et al., 2020).

As SEM images reveal, diatomite contains micro-pore structures with various shapes and sizes. The micro-pores are generally interconnected, creating a system of accessible openings for the transport of solutions and gases. Their existence shows low density of diagenetic processes in the siliceous clay mud.

Table 1. Chemical composition of PC and diatomite (wt%).

Materials	SiO_2	CaO	Al_2O_3	Fe_2O_3	MgO	SO_3	Na_2O	K_2O	Cl^-	Free CaO	Loss on ignition
PC	20.36	62.57	4.6	2.56	1.53	3.32	0.26	0.66	0.018	1.78	2.38
D	85.69	0.54	2.1	0.96	0.32	0.03	0.25	0.18	0.013	–	9.97

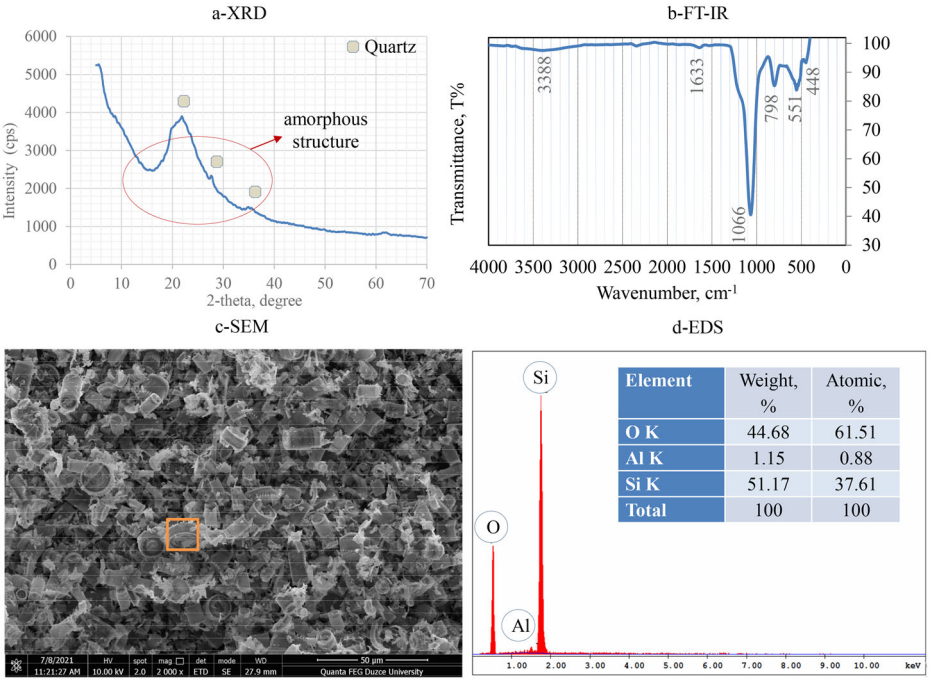

Figure 1. Images of XRD patterns (a), FT–IR diagram (b), SEM micrograph (c) and EDS spectra (d) of diatomite.

Table 2. Composition of cement mortars prepared in this study.

Mix.	PC, g	D, g	PC, %	D, %	Standart sand, g	w/b
R	450	0	100	0	1350	0.5
10D	405	45	90	10		0.55
20D	360	90	80	20		0.60

Intergranular micro-pores have irregular shapes due to their walls are composed by randomly spaced diatom frustules, corroded quartz and irregular accumulations of other mineral ingredients (Figure 1c) (Figarska-Warchoł et al., 2015). These micropores can be beneficial in terms of durability by decreasing microcracking due to autogenous shrinkage in cementitious materials. In addition, due to the porous adsorption feature of diatomite, it may be change the pore structure inside the material, thus increasing the resistance of the material to freezing (Sun et al., 2020).

Elemental analysis by EDS in micro fields on the diatomite surface indicates differences in the quantitative and qualitative chemical composition of the minerals. The EDS elemental analysis indicates that the most mainly elements are silicon and aluminum (Figure 1d). The elemental composition of diatomite obtained by EDS is compatible with the chemical composition (Table 1).

2.2. Samples preparation

The codes and mixing ratios used in the preparation of mortars are given in Table 2.

The mortars have been prepared correspondent with the requirements of TS EN 196-1 to determine compressive strength (TS EN 196-1, 2016). After the mortars were prepared, they were placed in three–-segmented moulds of size 4x4x16 cm immediately. The moulds placed shaking device, and the mortar was shaken in accordance with the requirements of standard. And then, the mortars were ameliorated in a laboratory at 20 ± 1 °C and 90% humidity for 24 hours. At the end of this period, it was taken out of the molds and put in the curing pool at 20 ± 1 °C up to the test days.

Cement pastes have been prepared in conceit with the requirements of TS EN 196-3 to determine water demand, setting time and volume expansion (TS EN 196-3, 2017). Considering the water demands,

cement pastes were produced with different w/b (water–binder) ratio of 0.35 for R, 0.42 for 10 D and 0.55 for 20 D for SEM/EDS, DTA/TGA, FT–IR and XRD. The produced cement pastes were poured into prepared molds to form 5x1x1 cm prisms. The paste samples were cured at 20 ± 1 °C and 90% relative humidity for 24 hours. The samples were then demolded and placed in water. The cement paste specimens were cured for 2, 7, 28 and 90 days, and then they were taken out of the water. The samples were dried in an oven at 60 °C for 2 hours. Then a piece of cement paste prism was taken and ground to a fine powder of <63 μm for DTA/TGA, FTIR and XRD. For SEM/EDS, another piece of cement paste prism was broken into cubes of 10 mm. Then the SEM image of broken sample was obtained.

2.3. Test methods

In the study, specific surface area (Blaine) with Toni Technik-Model 7202, specific weight with Quanta Chrome MVP–1 and sieve analysis with LSN-200 Hosokawa Alpine Air Jet Sieve devices of PC and diatomite were detected. Mineral phase analysis were performed with X-ray diffraction (Rikagu SmartLab XRD device) using Cu Kα ($\lambda = 1.54$ A°) radiation with the 2θ rang of 10° to 70°. FT–IR analysis were determined with Shimadzu (IRPrestige-21) Fourier Transform Infrared Spectrophotometer. DTA/TGA analysis were performed by means of Shimadzu DTG 60H–DSC 60 for phases identification under nitrogen atmosphere at a heating rate of 20 °C/min with temperature ranging from 20 °C to 1000 °C. SEM and EDS analysis was performed with FEI Quanta FEG 250 model device. The water demands and setting times of the pastes, in accordance with TS EN 196-3, were detected with Vicat's needle apparatus, and soundness of pastes was detected by Le Chatelier method (TS EN 196-3, 2017). The compressive strengths, correspondent with TS EN 196-1, were tested of cement mortars (TS EN 196-1, 2016). To determine compressive strengths, total six samples, which were later fractured halfway, for each each group were tested, and the average was the result.

3. Results and discussion

3.1. Water demand, setting time and volume expansion of pastes

Water demand, initial and final setting time and volume expansion of pastes are shown in Table 3.

Water demand varies according to its physical, chemical and mineralogical features of PC and diatomite. As seen from Table 2, water demands of pastes were significantly affected by increasing diatomite ratio in cement. In comparison to referance paste, water demands of the 10 D and 20 D pastes were increased 58% and 108%, respectively (Table 3). Because diatomite has a micro-pore structure in various shapes and sizes (Figure 1c) and a fine particle structure, it is thought that diatomite-substituted cement pastes need more water.

Expansions may occur due to reactions of the excessive amounts of magnesia, free lime and calcium sulfate within cement, and concrete may crack as a result. Le Chatelier's test to detect the volume expansion was conducted. As seen from Table 3, the volume expansion values were 1 mm. For this reason, it can be said that since no value is above 10 mm, which maximum value is offered by TS EN 196-3 (TS EN 196-3, 2017), it will not cause any problems in terms of expansion.

Setting time may vary depending on the specific surface area and the degree of hydration of the binder, the grain filling in the paste and the amount of water introduced into the system (Kapeluszna et al., 2021). Initial and final setting time of pastes were affected by increasing diatomite ratio in cement (Table 3). In comparison to referance paste, the initiative setting time of the 10 D and 20 D pastes were increased 13% and 25%, and the final setting time were increased 17% and 32%, respectively. The reason for this increase in setting time, which is obtained in accordance with the literature, is thought to be due to the pozzolanic activity, physical and chemical features of diatomite, and higher w/b ratio of diatomite-

Table 3. Water demand, setting time and volume expansion of pastes.

Mix.	Water demend, %	Initial setting time, min.	Final setting time, min.	Volume expansion, mm
R	26.5	160	205	1.0
10D	42.0	180	240	1.0
20D	55.0	200	270	1.0

replaced cement pastes compared to the reference cement paste (Genç, 2006; Gökkonca, 2010; Kapeluszna et al., 2021). According to these results, all pastes were found to have exceeded minimum initial setting time of 60 minutes for 42.5 R type PC (TS EN 197-1, 2002).

3.2. XRD patterns of the pastes

Figure 2 presents XRD patterns of the R, 10D and 20 D pastes at 2, 7, 28 and 90 days.

As seen as from Figure 2 that, the mainly crystallized hydration products for all the pastes are CH, C_3S, C_2S and AFt. The C-S-H gel is amorphous and therefore diffraction bands cannot be visualized in the XRD spectra (Lei et al., 2016). CH is a main hydration product of the R, 10 D and 20 D pastes at different ages, and the CH, a well-crystallized phase can be clearly identified. With the increase of age, it is clear that the CH content in all pastes gradually decreased due to the cement hydration. Nevertheless, the volume of CH caused by the pozzolanic reaction with the SiO_2 from the diatomite are decreased at 10 D and 20 D in comparison to the reference paste. This proves that diatomite-substituted cements consume more CH than PC at a later age and indicates the pozzolanic reactivity of the diatomite at the later stage of the cement hydration. Thus, more C–S–H and less CH amount are useful in order to enhance the mechanical features of 10 D and 20 D at later ages (Lei et al., 2016; Schöler et al., 2015; Zhao et al., 2021).

3.3. FT–IR spectra of the pastes

Figure 3 presents the FT–IR spectra of the R, 10 D and 20 D pastes at 2, 7, 28 and 90 days.

Because of the hydration products of pastes are chiefly amorphic C–S–H, FT–IR is often utilized to define the hydration products and their relative amounts by varying their typical wavenumbers and transmittance (Lei et al., 2016). In hydrated pastes, mainly mid bands in the range of 951–970 cm^{-1} are by in–plane Si–O bending and antisymmetric Si–O stretching vibrations in SiO_4 tetrahedra, which present C–S–H formation. Peaks within the range 1076–1110 cm^{-1} are corresponded to Si–O towing to the ettringite composition. C–O stretching in the range of 1389–1458 cm^{-1} and a weak shoulder band in the range of 802–866 cm^{-1} could be associated to are out–of–plane bending modes and anti–symmetric stretching of CO_3^{2-} ions, which are product resulting from carbonation. Bands within the range 1637–1652 cm^{-1} and 3373–3410 cm^{-1} could be associated to molecular water and O–H stretching, respectively. Wide absorption band in the scope of 2800–3700 cm^{-1} presents presence of $CaCO_3$, which represents a tendency of diminishing as hydration progresses. Bands at around 3591–3612 cm^{-1} of are assigned to O–H, and they are corresponded by the structure of CH (Figure 3) (Hidalgo et al., 2007; Huang et al., 2016; Lei et al., 2016; Sepehr et al., 2014). Compared the FT–IR bands of R, 10 D and 20 D pastes, the intensity of the bands in the scope of 947–970 cm^{-1} in 10 D and 20 D pastes appear to be slightly higher than the R

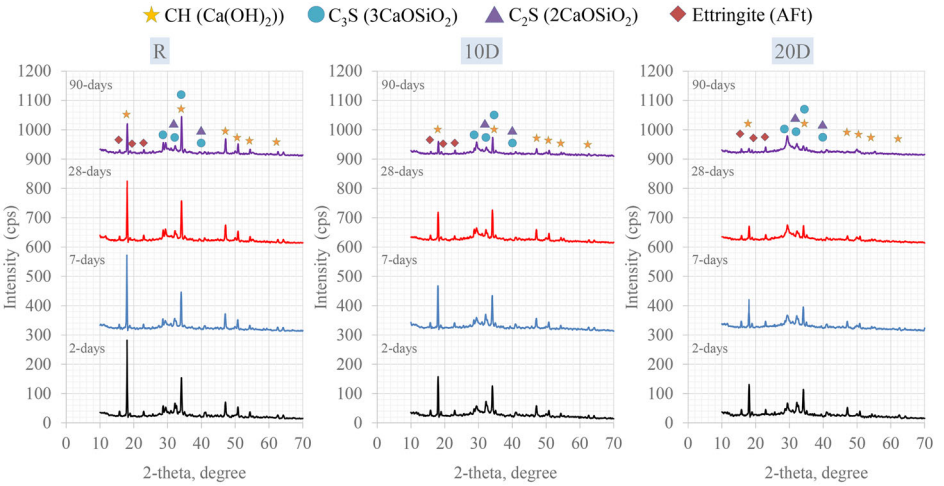

Figure 2. XRD patterns of pastes cured for 2, 7, 28 and 90 days.

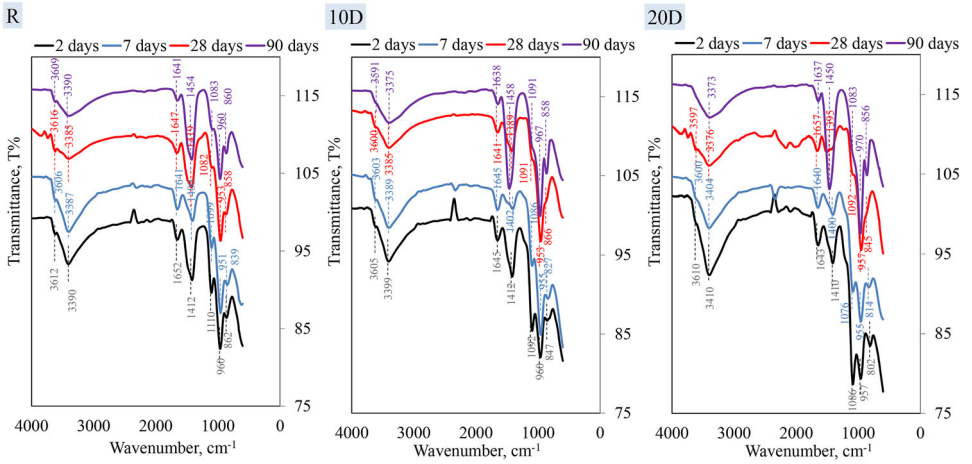

Figure 3. FT–IR diagram of pastes cured for 2, 7, 28 and 90 days.

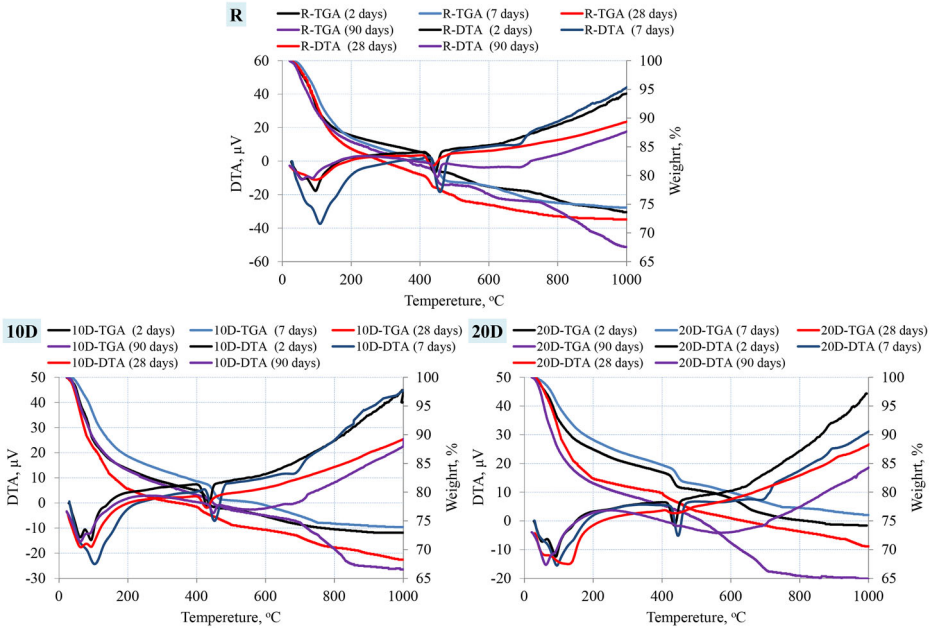

Figure 4. DTA–TGA patterns of pastes cured for 2, 7, 28 and 90 days.

at 90 hydration days. It can be concluded that the production of hydration outputs such as C-S-H will increase in 10 D and 20 D pastes at later ages (Lei et al., 2016). Moreover, 10 D and 20 D pastes indicates the lower intensity of CH bands in the range of 3591–3612 cm^{-1} than of R pastes. This can be explained by mens of pozzolanic reaction of pozzolana phases by CH that generated from hydration of cement phases (Saraya, 2014). In this context, the 10 D and 20 D pastes have the lowest CH band as a result of reaction of the amorphous silica reacting by CH to admixture mount of CSH, at later ages. Therefore, it can be said that the findings obtained by FT-IR analysis are compatible with the findings obtained by XRD analysis.

3.4. Thermal analysis of the pastes

Figure 4 presents DTA/TGA examination of the R, 10 D and 20 D pastes at 2, 7, 28 and 90 days.

The DTA curves present the presence of certain endothermic peaks at 41–160, 430–457 and 681–698 °C (Figure 4). The endothermic affects within the range 25–200 °C are caused with evaporation of free water, AFt and dehydration of C–S–H. Decomposition of CH causes endothermic effects in the 400–500 °C range temperature. The peak within the range 500–750 °C is indicated to the decomposition of $CaCO_3$ (Monteagudo et al., 2014; Saraya, 2014). Moreover, the weight loss between 105–1000 °C is determined as the chemically bonded water content. The weight loss that occurs in this temperature range is dehydration of cement hydration products such as portlandite, C–S–H gel and different hydrated products (Bhattacharya & Harish, 2018; Zhang et al., 2018). The weight losses in different temperature ranges, which are 25–200, 400–500, 500–750 and 105–1000 °C, calculated from TGA of pastes cured for 2, 7, 28 and 90 days are given in Figure 5.

The whole CH content in R, 10 D and 20 D pastes was obtained by the following equations.

$$\mathrm{CH}(\%) = \mathrm{a} * (74/18) + \mathrm{b} * (74/44) \quad (1)$$

where a and b represent weight losses caused by CH dehydration and $CaCO_3$ dissociation, respectively. 44, 18 and 74 are the molecular weight of CO_2, H_2O, and CH respectively (Bhattacharya & Harish, 2018; Zhang et al., 2018). Figure 6 shows the whole CH content.

As shown in Figure 5a, the amount of free water, C–S–H and AFt of the R pastes at 2, 7, 28 and 90 days are 13.0–13.4–15.4–14.1%; that in 10 D are 16.0–13.8–19.4–16.2%, in 20 D are 12.5–10.9–17.6–18.5%, respectively. The weight losses due to decomposition of $CaCO_3$ and dehydration of CH in R, 10 D and 20 D pastes at all curing ages are given in Figure 5b and c. The CH content at 2, 7, 28 and 90 days in R pastes calculated by the equation are 22.1–21.4– 20.5–19.4%; that in 10 D are 19.2–20.0–18.2–18.1%, and in 20 D are 20.7–20.4–18.1–17.3%, respectively (Figure 6). The chemically bound water content at 2, 7, 28 and 90 days in R pastes calculated via the equation are 17.5–19.1–19.2–23.1%; that in 10 D are 15.5–18.9–19.1–22.3%, and in 20 D are 17.9–18.5–19.0–21.5%, respectively (Figure 5d). According to these results, it is obvious that both with the increase of age and with the addition of diatomite, the CH content is reduced gradually. The findings obtained by TGA analysis are compatible with the findings obtained by XRD and FT-IR analysis. Furthermore, the weight percentage of chemically bound water of the diatomite substituted paste and the reference paste is almost

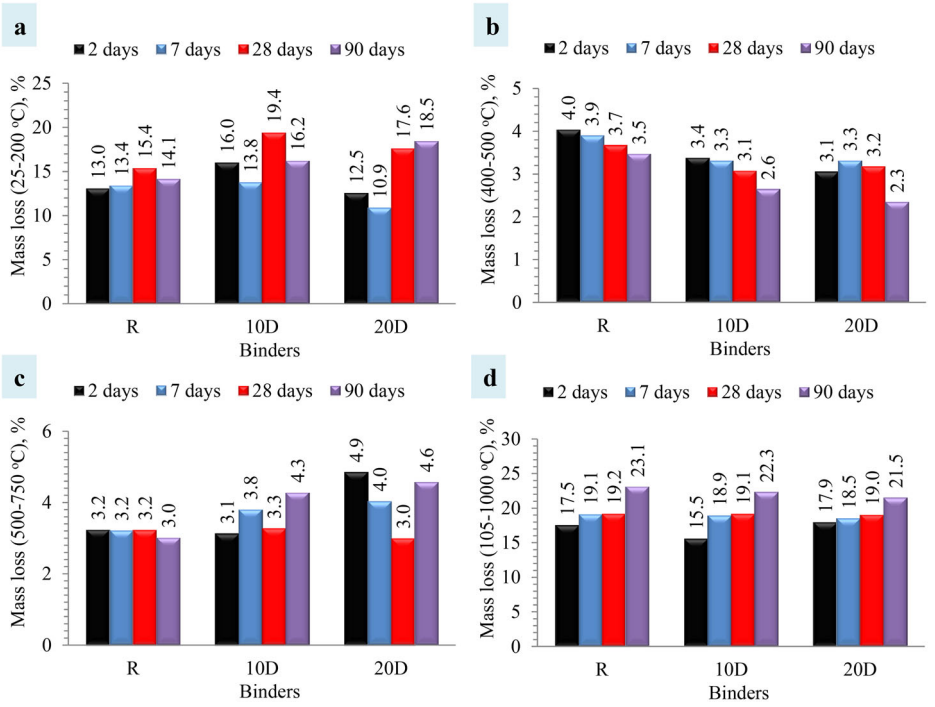

Figure 5. TGA result of pastes cured for 2, 7, 28 and 90 days.

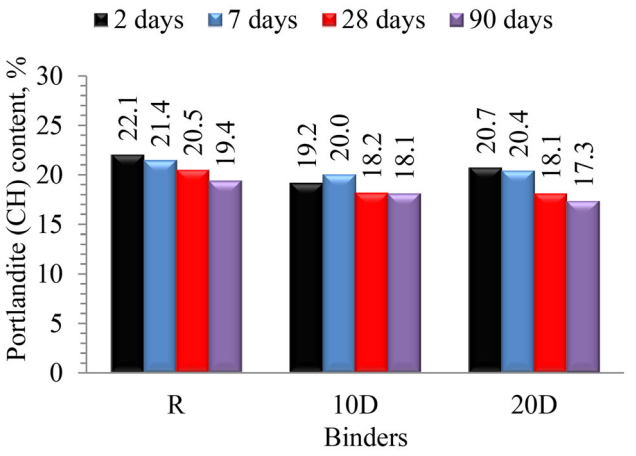

Figure 6. CH content in pastes for 2, 7, 28 and 90 days.

the same at 28 and 90 days. By taking this into account, perhaps more hydration products maybe formed and have a more compact structure in diatomite-substituted paste in later ages.

3.5. Microstructure analysis of the pastes

SEM footages of R, 10 D and 20 D pastes at 2, 7, 28 and 90 days are given in Figures 7–9, respectively.

As the hydration of R pastes at early ages, it may be seen in Figure 7 that the clinker grains were surrounded by radiating fibers of C-S-H. This morphology of C-S-H rich in lime seen in Figure 7a represents a relatively high porosity than pastes with pozzolan which have creased foils of C-S-H. At Figure 7a, Portlandite crystals are seen as the layered massive morphology. AFt crystals with stretched needle patterns were found in voids and cracks (Figure 7a). At 7 days, reticular mesh morphology is evident by bridging and interaction between grains (Figure 7b). EDS analysis show that the reticular network morphology are mainly composed of Ca and S for 2 days (Figure 7-1) and Ca, Si for 7 days (Figure 7-2), respectively. Figure 7c shows the classic interweaving of layered CH with C-S-H. EDS analysis shows that the structure is essentially composed of Ca (Figure 7-3). In 90 days, the featureless gel, which gives a certain stability to the structure by stuffing all the pores amid the particles, becomes predominant in the paste (Figure 7d). EDS examination reveals that the structure is primarily composed of Ca and Si (Figure 7-4) (Chen et al., 2018; Liu et al., 2020; Türker & Yeğinobalı, 2003).

Figures 8 and 9 present the SEM images of 10 D and 20 D pastes cured for 2, 7, 28 and 90 days. Diatomite has a highly porous microstructure, mainly in the form of disk-like and cylindrical shapes, and can significantly accelerate the formation of amorphous phases in early and later ages. At 2 and 7 days, it was observed that in pastes with 10% and 20% diatomite additive, the porosity increased when compared with Portland cement pastes. At these stages, the internal structure of the diatomite was filled with AFt and C–S–H, and CH was poorly defined. For this reason, it can be said that diatomite reacts with the cement matrix at an early age, and diatomite particles with finer and higher surface areas accelerate the formation of amorphous phases. In addition, EDS analysis of the 10 D paste reveals that the main elements are Ca, Si, Al and S for 2 days (Figur e8-1), and Ca, Al, Si and S for 7 days (Figure 8-2), respectively. The EDS analysis of the 20 D paste present that the mainly elements are Ca and Si for 2 days (Figure 9-1), and Si and Ca for 7 days (Figure 9-2), respectively. 10 D and 20 D pastes formed a thick construction at 28 days, and most of the spaces between diatomite and matrix filled by the structure of C–S–H (Figure 8c, 9d). The EDS spectrum on the surface of the diatomite particle in 10 D and 20 D paste reveals the development of the hydrated layer as rich in Ca, Si and Al (Figure 8-3), and Si and Ca (Figure 9-3), respectively. At 90 days, the coagulated gel morphology becomes predominant phase in the 10 D and 20 D paste and consolidated into a compact mass in which diatomite particles are embedded, as seen in Figures 8d and 9d. Thus, it can be stated that an increasingly high-strength dense structure emerges. The EDS analysis of the 10 D and 20 D paste present that the main elements are Ca and Si

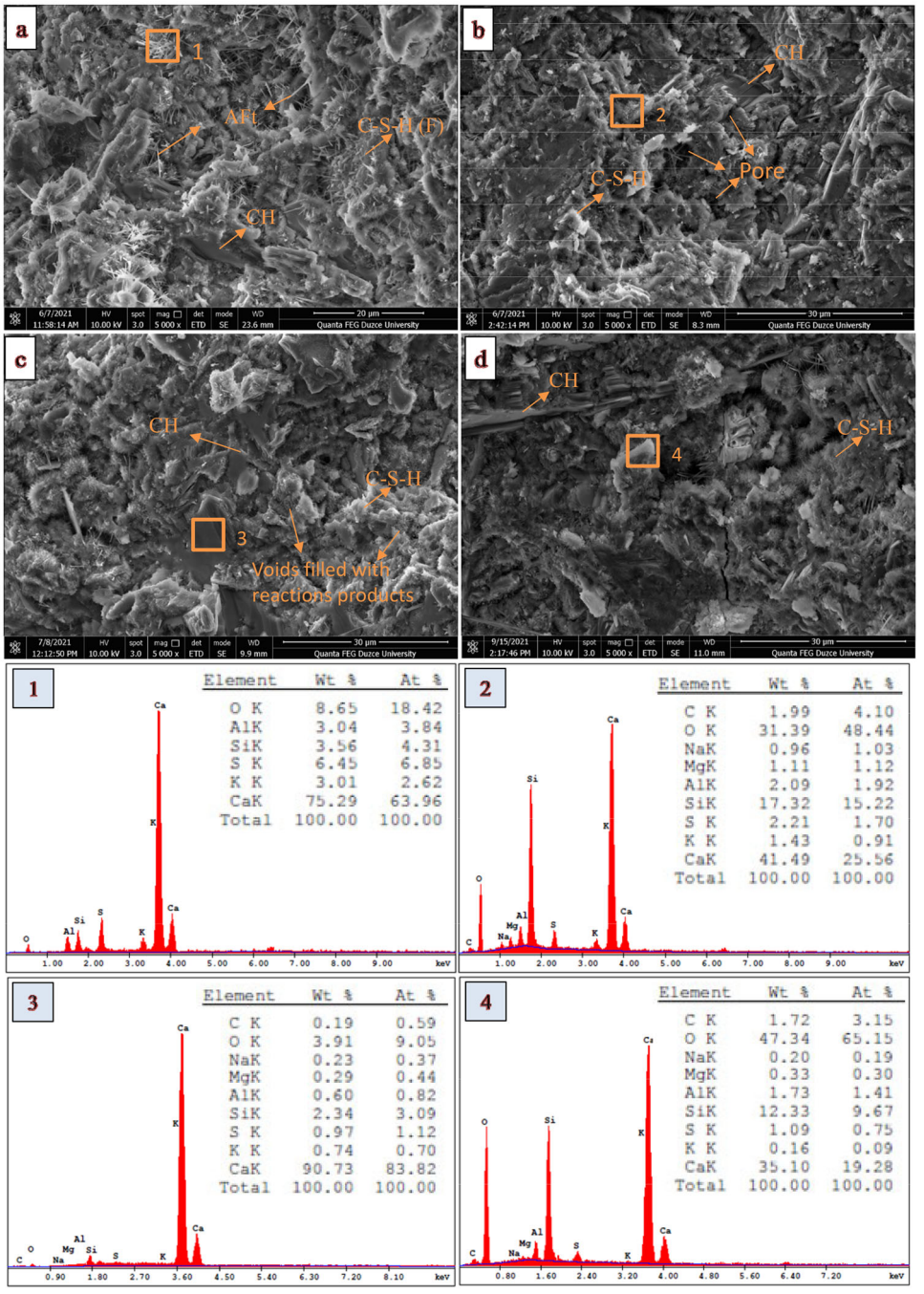

Figure 7. SEM images of R pastes cured for 2 (a), 7 (b), 28 (c) and 90 days (d).

(Figure 8-4), and Ca, Al and Si (Figure 9-4), respectively (Chen et al., 2018; Liu et al., 2020; Türker & Yeğinobalı, 2003).

When SEM images are evaluated in general, the principal hydration products of pastes are AFt, CH and C–S–H gels, and it can be said that as the hydration age increases, diatomite substituted pastes have a denser microstructure than reference pastes.

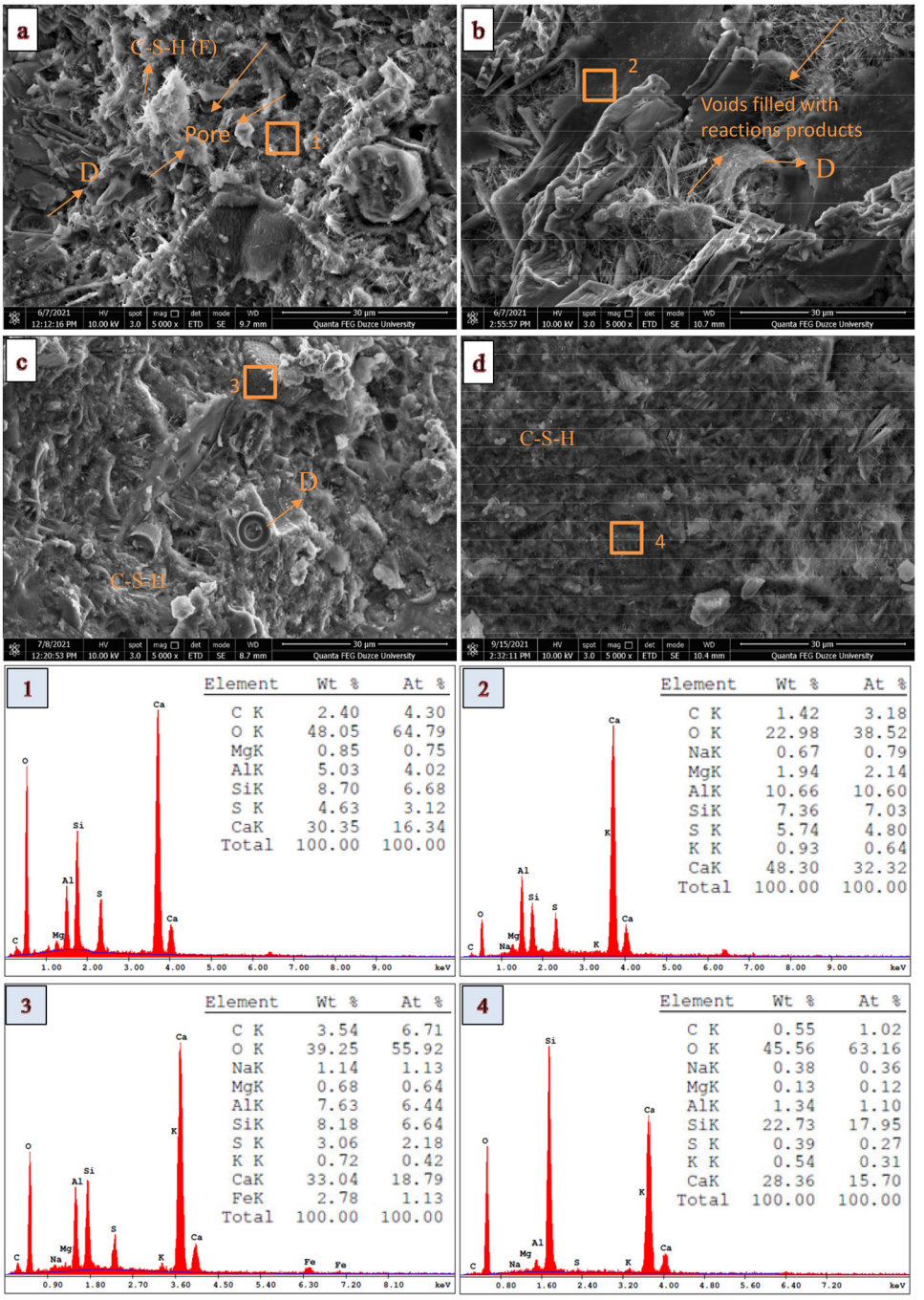

Figure 8. SEM images of 10 D pastes cured for 2 (a), 7 (b), 28 (c) and 90 days (d).

3.6. Compressive strength

Figure 10 presents the compressive strength of mortars at 2, 7, 28 and 90 days.

As shown in Figure 10, mortars produced by PC presented the highest compressive strength at all curing ages, reaching 30.8, 43.6, 54.7 and 60.0 MPa at 2, 7, 28 and 90 days, respectively. The compressive strengths of mortars with 10% diatomite substitution reduced by 26.0%, 21.2%, 5.8% and 2.0% after curing for 2, 7, 28 and 90 days, respectively, compared with the reference mortars. With 20% diatomite

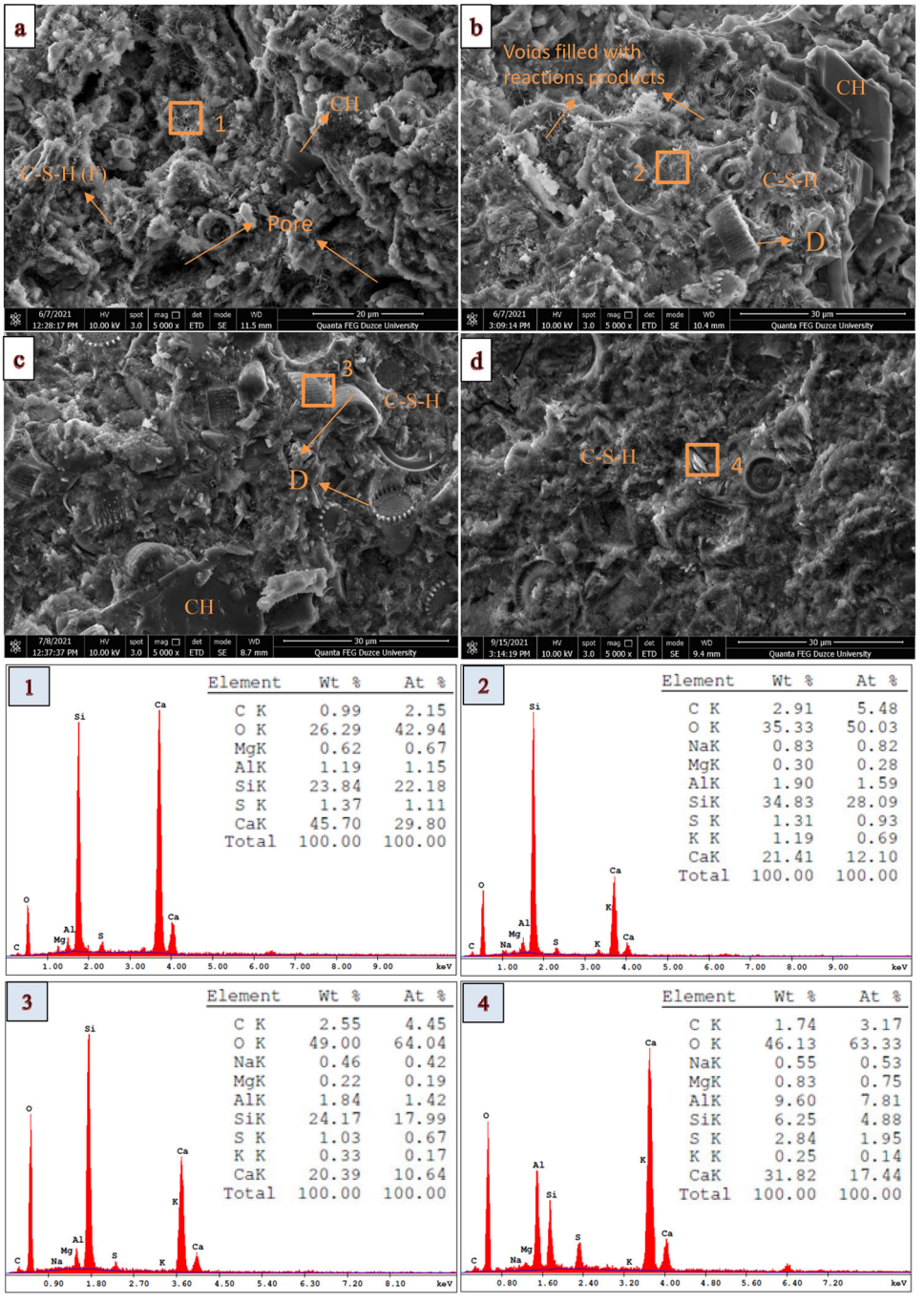

Figure 9. SEM images of 20 D pastes cured for 2 (a), 7 (b), 28 (c) and 90 days (d).

substitution to PC, the compressive strengths of the mortars produced decreased by 41.9%, 41.0%, 16.2% and 16.3% after curing for 2, 7, 28 and 90 days, respectively, compared with the reference mortars. The negative effects on the compressive strengths due to diatomite substitution decreased at later age. The reason for this is stated that the AFt formation determines the compressive strength development in cement in the early hydration periods, diatomite is more liable to be adsorbed onto the aluminate minerals (C_3A and C_4AF), restricting the formation of AFt, and lead to lower early ages compressive strength

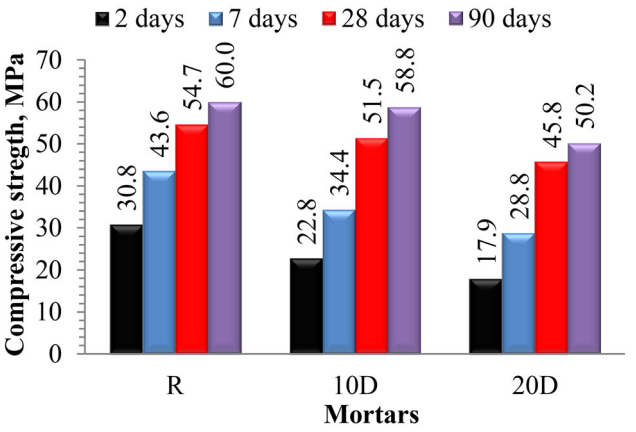

Figure 10. Compressive strength of the mortars cured for 2, 7, 28 and 90 days.

(Zhao et al., 2021). By contrast, the diatomite with high specific surface area, consumes more CH to create C–S–H gel at later age (Figure 5), resulting in a denser microstructure than R paste (Figures 8–10). And also, the chemically bound water content of diatomite-substituted pastes at 90 days is almost the same as in R paste (Figure 5d). All these reactions lead to diatomite-substituted mortars a continuous increase in compressive strength especially in later ages. According to the findings obtained, it is obvious that 90 days compressive strength almost reaches to the reference mortar with the content of 10% diatomite. Furthermore, the compressive strength values at the end of 28 days of all mortars with 10% and 20% diatomite were obtained above the minimum value of 42.5 MPa (Figure 10). According to this result, it can be said that may be achieved save up to 20% of PC.

4. Conclusions

In this study, standard cement experiments were used to assess the setting period, water requirement, and volume expansion of PC and diatomite-substituted cement pastes. Furthermore, effects of diatomite on compressive strength and hydration reactions by technics such as XRD, FT–IR, DTA/TGA, SEM/EDS, were investigated at 2, 7, 28 and 90 days. According to the findings:

- Water demand for normal consistency was increased with increasing diatomite content.
- The volume expansion and initial setting period values of referance and diatomite-substituted pastes are in accordance with the value limited by the standards.
- The XRD, TGA and SEM data suggest that the diatomite–containing cement has a high hydration degree at an early age and will continue to hydrate. Furthermore, at 90 days, the chemically bonded water content in 10D paste is equivalent to PC. This shows that diatomite-replaced cement paste may have a more compact structure by forming more hydration products at later ages.
- The principal hydration products of pastes, according to SEM figures, are AFt, CH and C–S–H gels. In addition, as the hydration age increases, diatomite-substituted pastes have a denser microstructure than reference pastes.
- While diatomite-substituted mortars show a significant loss in compressive strength especially at 2 and 7 days, it exhibits a continuous increase at 28 and 90 days.
- Compressive strength values at the end of 28 days of 10% and 20% diatomite-substituted mortars were found to be higher than the minimum value of 42.5 MPa for CEM I 42.5 R type cement in the TS EN 197-1 standard. Therefore, it will provide economic (energy-saving) and ecological advantages by saving up to 20% as a result of the reduction in the manufacture of Portland cement.

When the results are evaluated in general, it can be stated that raw diatomite can be used to produce a green and environmentally friendly cement-based material in terms of both mechanical and durability.

Disclosure statement

The authors indicate that they have no known personal relationships or competing financial interests that could have appeared to influence the work reported in the manuscript.

Funding

This work was supported via Düzce University Research Fund (Project Code No: 2021.06.08.1190). Furthermore, the authors gratefully acknowledge CIMSA cement factory (Turkey-Eskişehir) managers and employees for their invaluable contributions to this work.

References

Ahmadi, Z., Esmaeili, J., Kasaei, J., & Hajialioghli, R. (2018). Properties of sustainable cement mortars containing high volume of raw diatomite. *Sustainable Materials and Technologies*, *16*, 47–53. https://doi.org/10.1016/j.susmat.2018.05.001

Akbarpour, A., & Mahdikhani, M. (2022). Effects of natural zeolite and sulfate environment on mechanical properties and permeability of cement–bentonite cutoff wall. *European Journal of Environmental and Civil Engineering*, 1–14. https://doi.org/10.1080/19648189.2022.2075940

Ashraf, M., Iqbal, M. F., Rauf, M., Ashraf, M. U., Ulhaq, A., Muhammad, H., & Liu, Q. F. (2022). Developing a sustainable concrete incorporating bentonite clay and silica fume: Mechanical and durability performance. *Journal of Cleaner Production*, *337*, 130315. https://doi.org/10.1016/j.jclepro.2021.130315

ASTM C618. (2003). *Standard specification for coal fly ash and raw or calcined natural pozzolan for use in concrete*. American society for testing and materials.

Bhattacharya, M., & Harish, K. V. (2018). An integrated approach for studying the hydration of portland cement systems containing silica fume. *Construction and Building Materials*, *188*, 1179–1192. https://doi.org/10.1016/j.conbuildmat.2018.08.114

Chen, X., Zhou, M., Shen, W., Zhu, G., & Ge, X. (2018). Mechanical properties and microstructure of metakaolin-based geopolymer compound-modified by polyacrylic emulsion and polypropylene fibers. *Construction and Building Materials*, *190*, 680–690. https://doi.org/10.1016/j.conbuildmat.2018.09.116

Costa, J. A. C., Martinelli, A. E., do Nascimento, R. M., & Mendes, A. M. (2020). Microstructural design and thermal characterization of composite diatomite-vermiculite paraffin-based form-stable PCM for cementitious mortars. *Construction and Building Materials*, *232*, 117167. https://doi.org/10.1016/j.conbuildmat.2019.117167

Degirmenci, N., & Yilmaz, A. (2009). Use of diatomite as partial replacement for Portland cement in cement mortars. *Construction and Building Materials*, *23*(1), 284–288. https://doi.org/10.1016/j.conbuildmat.2007.12.008

Figarska-Warchoł, B., Stańczak, G., Rembiś, M., & Toboła, T. (2015). Diatomaceous rocks of the Jawornik deposit (the Polish Outer Carpathians): Petrophysical and petrographical evaluation. *Geology, Geophysics & Environment*, *41*(4), 311–331. https://doi.org/10.7494/geol.2015.41.4.311

Ganeshan, M., & Venkataraman, S. (2021). Durability and microstructural studies on fly ash blended self-compacting geopolymer concrete. *European Journal of Environmental and Civil Engineering*, *25*(11), 2074–2088. https://www.tandfonline.com/loi/tece20. https://doi.org/10.1080/19648189.2019.1615991

Genç, S. S. (2006). *The characteristics of the behaviour and usebility of concrete with diatomite under load* [Master's thesis, Graduate School of Natural and Applied Sciences, Ondokuzmayıs University].

Gerengi, H., Kocak, Y., Jazdzewska, A., & Kurtay, M. (2017). Corrosion behavior of concrete produced with diatomite and zeolite exposed to chlorides. *Computers and Concrete*, *19*(2), 161–169. https://doi.org/10.12989/cac.2017.19.2.161

Gökkonca, E. K. (2010). *Analysing mortar's some mechanical and physical characteristics changes additive with diatomites* [Master's thesis, Graduate School of Natural and Applied Sciences, Pamukkale University].

Hasanbeigi, A., Price, L., & Lin, E. (2012). Emerging energy-efficiency and CO2 emission-reduction technologies for cement and concrete production: A technical review. *Renewable and Sustainable Energy Reviews*, *16*(8), 6220–6238. https://doi.org/10.1016/j.rser.2012.07.019

Hidalgo, A., Petit, S., Domingo, C., Alonso, C., & Andrade, C. (2007). Microstructural characterization of leaching effects in cement pastes due to neutralisation of their alkaline nature: Part I: Portland cement pastes. *Cement and Concrete Research*, *37*(1), 63–70. https://doi.org/10.1016/j.cemconres.2006.10.002

Huang, X., Jiang, M., Zhao, X., & Tang, C. (2016). Mechanical properties and hydration mechanisms of high-strength fluorogypsum-blast furnace slag-based hydraulic cementitious binder. *Construction and Building Materials*, *127*, 137–143. https://doi.org/10.1016/j.conbuildmat.2016.09.152

Kapeluszna, E., Szudek, W., Wolka, P., & Zieliński, A. (2021). Implementation of alternative mineral additives in low-emission sustainable cement composites. *Materials*, *14*(21), 6423. https://doi.org/10.3390/ma14216423

Kastis, D., Kakali, G., Tsivilis, S., & Stamatakis, M. G. (2006). Properties and hydration of blended cements with calcareous diatomite. *Cement and Concrete Research*, *36*(10), 1821–1826. https://doi.org/10.1016/j.cemconres.2006.05.005

Kocak, Y. (2017). The effects of super plasticizer and trass on the cement hydration. *Pamukkale University Journal of Engineering Sciences*, *23*(3), 184–192. https://doi.org/10.5505/pajes.2016.80008

Kocak, Y. (2020). Effects of metakaolin on the hydration development of Portland–composite cement. *Journal of Building Engineering*, *31*, 101419. https://doi.org/10.1016/j.jobe.2020.101419

Kurtay, M., Gerengi, H., Kocak, Y., Chidiebere, M. A., & Yildiz, M. (2020). The potency of zeolite and diatomite on the corrosive destruction of reinforcing steel in 1 M HNO3 environment. *Construction and Building Materials*, *236*, 117572. https://doi.org/10.1016/j.conbuildmat.2019.117572

Lauermannová, A.-M., Lojka, M., Jankovský, O., Faltysová, I., Pavlíková, M., Pivák, A., Záleská, M., & Pavlík, Z. (2021). High-performance magnesium oxychloride composites with silica sand and diatomite. *Journal of Materials Research and Technology*, *11*, 957–969. https://doi.org/10.1016/j.jmrt.2021.01.028

Lei, D. Y., Guo, L. P., Sun, W., Liu, J., Shu, X., & Guo, X. L. (2016). A new dispersing method on silica fume and its influence on the performance of cement-based materials. *Construction and Building Materials*, *115*, 716–726. https://doi.org/10.1016/j.conbuildmat.2016.04.023

Lei, L., & Zhang, Y. (2021). Preparation of isoprenol ether-based polycarboxylate superplasticizers with exceptional dispersing power in alkali-activated slag: Comparison with ordinary Portland cement. *Composites Part B: Engineering*, *223*, 109077. https://doi.org/10.1016/j.compositesb.2021.109077

Lenka, B. P., Majhi, R. K., Singh, S., & Nayak, A. N. (2022). Eco-friendly and cost-effective concrete utilizing high-volume blast furnace slag and demolition waste with lime. *European Journal of Environmental and Civil Engineering*, *26*(11), 5351–5373. https://doi.org/10.1080/19648189.2021.1896581

Li, J., Zhang, W., Li, C., & Monteiro, P. J. (2019). Green concrete containing diatomaceous earth and limestone: Workability, mechanical properties, and life-cycle assessment. *Journal of Cleaner Production*, *223*, 662–679. https://doi.org/10.1016/j.jclepro.2019.03.077

Liu, J., Qin, Q., & Yu, Q. (2020). The effect of size distribution of slag particles obtained in dry granulation on blast furnace slag cement strength. *Powder Technology*, *362*, 32–36. https://doi.org/10.1016/j.powtec.2019.11.115

Liu, J., Wu, K., Wang, Y., & Yang, Y. (2017). Effects of fly ash/diatomite admixture with variable particle sizes on the mechanical properties and porosity of concrete. *Journal of Wuhan University of Technology-Mater. Sci. Ed*, *32*(5), 1072–1079. https://doi.org/10.1007/s11595-017-1713-8

Liu, R., Yang, Y., Zhao, X., & Pang, B. (2021). Quantitative phase analysis and microstructural characterization of Portland cement blends with diatomite waste using the Rietveld method. *Journal of Materials Science*, *56*(2), 1242–1254. https://doi.org/10.1007/s10853-020-05429-1

Mastali, M., & Dalvand, A. (2018). The impact resistance and mechanical properties of fiber reinforced self-compacting concrete (SCC) containing nano-SiO2 and silica fume. *European Journal of Environmental and Civil Engineering*, *22*(1), 1–27. https://doi.org/10.1080/19648189.2016.1177604

Monteagudo, S. M., Moragues, A., Gálvez, J. C., Casati, M. J., & Reyes, E. (2014). The degree of hydration assessment of blended cement pastes by differential thermal and thermogravimetric analysis. *Thermochimica Acta*, *592*, 37–51. https://doi.org/10.1016/j.tca.2014.08.008

Paiva, H., Silva, A. S., Velosa, A., Cachim, P., & Ferreira, V. M. (2017). Microstructure and hardened state properties on pozzolan-containing concrete. *Construction and Building Materials*, *140*, 374–384. https://doi.org/10.1016/j.conbuildmat.2017.02.120

Pınarcı, İ., & Kocak, Y. (2022). Hydration mechanisms and mechanical properties of pumice substituted cementitious binder. *Construction and Building Materials*, *335*, 127528. https://doi.org/10.1016/j.conbuildmat.2022.127528

Pokorny, J., Zaleska, M., Pavlikova, M., & Pavlik, Z. (2019). Properties of fine-grained concrete with admixture of diatomite powder. *IOP Conference Series: Materials Science and Engineering*, *603*(2), 022045. https://doi.org/10.1088/1757-899X/603/2/022045

Qian, T., Li, J., Min, X., Deng, Y., Guan, W., & Ning, L. (2015). Diatomite: A promising natural candidate as carrier material for low, middle and high temperature phase change material. *Energy Conversion and Management*, *98*, 34–45. https://doi.org/10.1016/j.enconman.2015.03.071

Sandhu, R. K., & Siddique, R. (2022). Properties of sustainable self-compacting concrete made with rice husk ash. *European Journal of Environmental and Civil Engineering*, *26*(13), 6670–6694. https://doi.org/10.1080/19648189.2021.1955747

Saraya, M. E. S. I. (2014). Study physico-chemical properties of blended cements containing fixed amount of silica fume, blast furnace slag, basalt and limestone, a comparative study. *Construction and Building Materials*, *72*, 104–112. https://doi.org/10.1016/j.conbuildmat.2014.08.071

Sarı, A., Hekimoğlu, G., Tyagi, V. V., & Sharma, R. K. (2020). Evaluation of pumice for development of low-cost and energy-efficient composite phase change materials and lab-scale thermoregulation performances of its cementitious plasters. *Energy*, *207*, 118242. https://doi.org/10.1016/j.energy.2020.118242

Schöler, A., Lothenbach, B., Winnefeld, F., & Zajac, M. (2015). Hydration of quaternary Portland cement blends containing blast-furnace slag, siliceous fly ash and limestone powder. *Cement and Concrete Composites*, *55*, 374–382. https://doi.org/10.1016/j.cemconcomp.2014.10.001

Sepehr, M. N., Amrane, A., Karimaian, K. A., Zarrabi, M., & Ghaffari, H. R. (2014). Potential of waste pumice and surface modified pumice for hexavalent chromium removal: Characterization, equilibrium, thermodynamic and kinetic study. *Journal of the Taiwan Institute of Chemical Engineers*, *45*(2), 635–647. https://doi.org/10.1016/j.jtice.2013.07.005

Sun, M., Zou, C., & Xin, D. (2020). Pore structure evolution mechanism of cement mortar containing diatomite subjected to freeze-thaw cycles by multifractal analysis. *Cement and Concrete Composites*, *114*, 103731. https://doi.org/10.1016/j.cemconcomp.2020.103731

Tran, Y. T., Lee, J., Kumar, P., Kim, K. H., & Lee, S. S. (2019). Natural zeolite and its application in concrete composite production. *Composites Part B: Engineering*, *165*, 354–364. https://doi.org/10.1016/j.compositesb.2018.12.084

TS 25. (2015). *Natural pozzolan (Trass) for use in cement and concrete - Definitions, requirements and conformity criteria*. Turkish Standards.

TS EN 196-1. (2016). *Methods of testing cement–Part 1: Determination of strength*. Turkish Standards.

TS EN 196-3. (2017). *Methods of testing cement–Part 3: Determination of setting time and soundness*. Turkish Standards.

TS EN 197-1. (2002). *Cement– Part 1: Compositions and conformity criteria for common cements*. Turkish Standards.

Türker, P., & Yeğinobalı, A. (2003). Comparison of hydration products of different pozzolanic systems. *Cement and Concrete World*, *46*, 52–66.

Wen, R., Zhang, X., Huang, Z., Fang, M., Liu, Y., Wu, X., Min, X., Gao, W., & Huang, S. (2018). Preparation and thermal properties of fatty acid/diatomite form-stable composite phase change material for thermal energy storage. *Solar Energy Materials and Solar Cells*, *178*, 273–279. https://doi.org/10.1016/j.solmat.2018.01.032

Yao, G., Lei, J., Zhang, X., Sun, Z., Zheng, S., & Komarneni, S. (2018). Mechanism of zeolite X crystallization from diatomite. *Materials Research Bulletin*, *107*, 132–138. https://doi.org/10.1016/j.materresbull.2018.07.021

Zhang, B., Tan, H., Shen, W., Xu, G., Ma, B., & Ji, X. (2018). Nano-silica and silica fume modified cement mortar used as Surface Protection Material to enhance the impermeability. *Cement and Concrete Composites*, *92*, 7–17. https://doi.org/10.1016/j.cemconcomp.2018.05.012

Zhao, Y., Gao, J., Xu, Z., Li, S., Luo, X., & Chen, G. (2021). Long-term hydration and microstructure evolution of blended cement containing ground granulated blast furnace slag and waste clay brick. *Cement and Concrete Composites*, *118*, 103982. https://doi.org/10.1016/j.cemconcomp.2021.103982